small
NANO MICRO

'Fairy Chimney'-Shaped Tandem Metamaterials as Double Resonance SERS Substrates

Neval A. Cinel, Serkan Bütün, Gülay Ertaş, and Ekmel Özbay*

***A** highly tunable design for obtaining double resonance substrates to be used in surface-enhanced Raman spectroscopy is proposed. Tandem truncated nanocones composed of Au-SiO_2-Au layers are designed, simulated and fabricated to obtain resonances at laser excitation and Stokes frequencies. Surface-enhanced Raman scattering experiments are conducted to compare the enhancements obtained from double resonance substrates to those obtained from single resonance gold truncated nanocones. The best enhancement factor obtained using the new design is 3.86×10^7. The resultant tandem structures are named after "Fairy Chimneys" rock formation in Cappadocia, Turkey.*

1. Introduction

Surface-enhanced Raman scattering (SERS) has been widely studied since its discovery in 1977.[1,2] There have been many debates regarding its origin to be electromagnetic and/or chemical. According to the widely accepted compromise the SERS is mainly caused by the electromagnetic contribution whereas the chemical mechanism due to charge-transfer resonances have a minor effect to the total enhancement factor on the order of 10–100.[3–6]

N. A. Cinel
Nanotechnology Research Center
Department of Electrical and Electronics Engineering
Bilkent University
06800 Bilkent, Turkey
E-mail: nyilmaz@ee.bilkent.edu.tr
Dr. S. Bütün
Department of Electrical Engineering and Computer Science
Northwestern University
60208, Evanston, IL, USA
Prof. G. Ertaş
Department of Chemistry
Middle East Technical University
06800 Ankara, Turkey
Prof. E. Özbay
Nanotechnology Research Center
Department of Electrical and Electronics Engineering
Department of Physics
Bilkent University
06800 Bilkent, Turkey

DOI: 10.1002/smll.201201286

Plasmonics is a new branch of photonics that deals with interaction of light with matter in metallic nanostructures.[7] Surface plasmons are the electromagnetic waves that exist at metal-dielectric interfaces, caused by the collective motion of valence electrons in the metal. They are named as localized surface plasmons (LSPs) when they are confined to metallic nano scale structures. The electromagnetic mechanism of SERS originates from the excitation of LSPs due to the interaction of light with metallic nanostructures (nano-roughened surfaces, in general). The excitation of LSPs ends up with the generation of strong electromagnetic fields that leads to enhanced inelastic scattering known as SERS.

Several methods have been used to exploit the relation between LSPR and SERS. In plasmon-sampled surface-enhanced Raman excitation spectroscopy (PS-SERES) method, samples with different LSPR extinction maxima are illuminated with the same excitation laser and then their respective SERS enhancement factors (EFs) are compared whereas in wavelength-scanned surface-enhanced Raman excitation spectroscopy (WS-SERES) the SER spectra from a single substrate is obtained with the use of many laser excitation wavelengths.[8,9] Both approaches showed that there is a strong correlation between SERS and LSP resonance. In the work of Haynes,[8] the maximum SERS enhancement was reported for excitation frequencies that are slightly blue-shifted with respect to the LSP resonance frequency. Among the vibrational modes of the molecule under study, the Raman shifted peak closer to the LSP resonance frequency ended with a larger enhancement than that of a farther Raman shifted peak. In the work of McFarland,[9] it is stated

that the maximum SERS EF occurs when the LSP resonance frequency is located in between the excitation and Stokes frequencies so that both the incident photon and the Raman scattered photon are strongly enhanced.

SERS EF is influenced from the particle near-field enhancement at the incident (excitation) wavelength and the re-radiation of the Raman signal emitted at the near field of the nanostructures at Stokes wavelength.[10,11] Therefore, double resonance designs can provide increased enhancement when the resonances are properly tuned to the excitation and the Stokes frequencies respectively. This can be summarized using Equation 1. Here, "E_{loc}" and "E_0" stands for the local and the incident electric fields, respectively. λ_{exc} refers to excitation wavelength and λ_{stokes} is the Stokes wavelength.[12]

$$G_{SERS} \propto \left| \frac{E_{loc}\ (\lambda_{exc})\ E_{loc}\ (\lambda_{stokes})}{E_0\ (\lambda_{exc})\ E_0\ (\lambda_{stokes})} \right|^2 = g\ (\lambda_{exc})\ g\ (\lambda_{stokes}) \qquad (1)$$

Recently, there have been some reports that investigate the double resonance structures as SERS substrates.[13,14] In the work of Chu,[13] the design includes a metallic nano-disk array separated from a gold film by a dielectric spacer. The surface plasmon polariton on the gold film interacts with the LSPR of the metallic array and double resonance characteristics is observed in optical transmission measurements. In the work of Banaee,[14] "in-plane" nano-particle pairs are used to obtain the plasmonic coupling. In the current study, we propose a different way to achieve plasmonic coupling by aligning the nanostructures in the light propagation direction which would end up with a better spatial overlap. Tandem Au-SiO_2-Au truncated nanocones designed this way, offer a highly tunable means to obtain the desired resonance frequencies. Their transmission spectra exhibit two separate and tunable transmission dips associated with hybridized modes resulting from the dipolar coupling between the metallic layers split with a dielectric spacer. Similar tandem metamaterial structures reported in literature include 2D arrays of Al-Al_2O_3-Al nanoparticle pairs and Au-MgF_2-Au nanoparticle pairs on quartz substrates fabricated using extreme-UV interference lithography (EUV-IL).[15,16] However their strong near-field coupling is shown to increase SERS enhancement firstly in this study. The best SERS EF obtained from tandem double resonance substrates in this study is in the same order with the work of Chu.[13] Double resonance substrates provided a roughly 10 fold increase in EF than their single resonance counter-parts.

Double resonance structures may prove to be useful in several applications such as NIR-SERS which can help overcome the disadvantages of visible lasers such as photochemical reactions, background from fluorescence and degeneration of molecules.[17,18] Since the excitation and Stokes shifted wavelengths can be more than 200 nm apart from each other in NIR-SERS, a single resonance structure can not provide enhancement at both wavelengths. This can be circumvented with the use of properly tuned double resonance structures as described in this report.

Another application can be Surface Enhanced Hyper Raman Scattering (SEHRS). SEHRS can provide vibrational information on molecules where ordinary Raman Scattering is suppressed and it is much more sensitive to local surface environmental changes than SERS.[19] The scattering signal in SEHRS follow the rule $w = 2w_0 - \Delta w$, where $2w_0$ is the second harmonic of the excitation frequency and Δw is the vibrational frequency. In this case the two resonances should be located at w_0 and $2w_0$ as also suggested in previous reports.[14]

2. Results and Discussion

2.1. Double Resonance Substrate Fabrication and Design

The SERS-active roughened surfaces can be fabricated by several methods like oxidation-reduction cycling, metal colloids, cold deposited films, island films and lithography. Since LSPR is highly dependent on the size and shape of the nanoparticles, lithographically prepared surfaces provide the most predictable and reproducible substrates whose resonances can be tuned easily.[6] Lithographically prepared nano structure designs can also be simulated accurately which reduces fabrication efforts. The enhancement factor calculation is more reliable due to more accurate estimations of physical dimensions, too. In this study we have fabricated our SERS-active substrates using electron beam lithography which produces highly reproducible nano-particle arrays with uniform shapes and size distributions.[20]

The substrate is composed of several sensor areas of 50 μm × 50 μm that contains different sized nano-arrays. The sizes of individual nano-particles are varied by changing the exposure dose of electron beam. Due to the self shadowing effect during metal-evaporation the nanostructures are shaped into truncated cones. The resultant shapes resembles and named after "Fairy Chimneys" rock formations found in Cappadocia, Turkey.[21] The size, shape and period of the nano-particles are investigated by scanning electron microscope (SEM). The cone angle is determined as θ~20 ± 2°. The period of the resultant arrays are 200 nm, radii ranges from 35 nm to 60 nm. The metal thicknesses are 30 nm-15 nm-30 nm for Au-SiO_2-Au layers, respectively. The SEM images taken from various sensor areas are shown in **Figure 1**a-b.

For comparison of Au-SiO_2-Au tandem structures exhibiting double resonance behavior to gold structures exhibiting single resonance behavior another sample is prepared following the same procedure as described in Experimental Section. The sensor areas that have their resonance at the same wavelength with the electrical resonance of double resonance structures are selected for comparison.

2.2. Optical Transmission Measurements

The optical characteristics of the tandem structures are studied using a custom spectral transmission setup. Light is transmitted by a multimode optical fiber to a lens that illuminates the biosensor through a collimating lens that collects the light at the input. The light is then transmitted through the biosensor and collected by the imaging lens. The image is projected onto an aperture that enables only the signal from the selected region on the measured sample to be transmitted. Another focusing lens couples this signal to the

small NANO MICRO

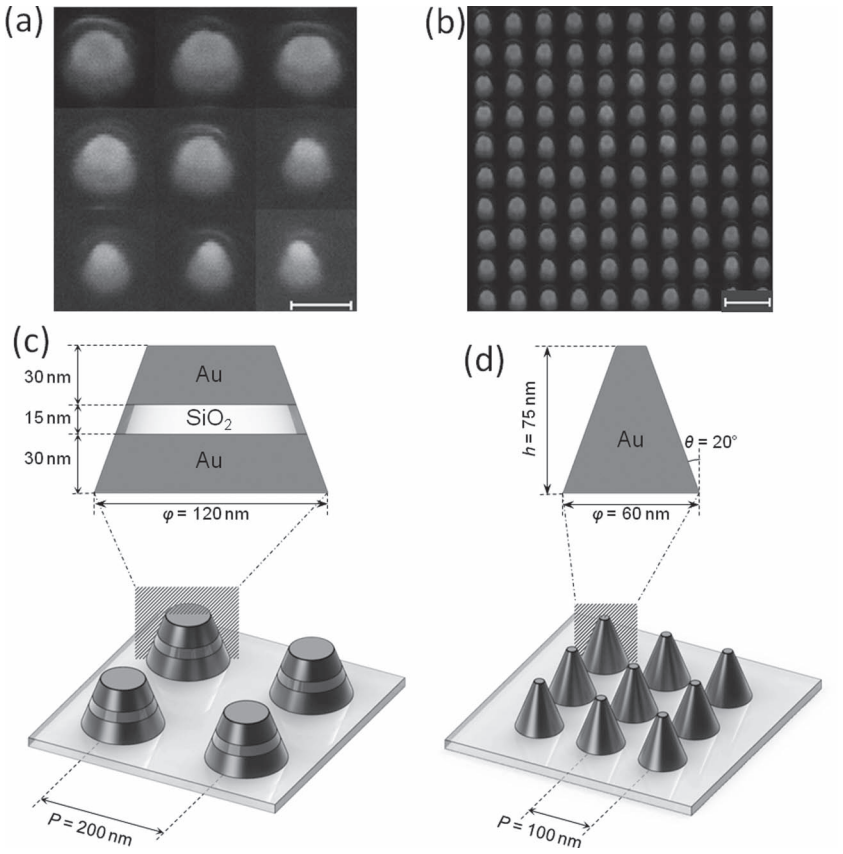

Figure 1. The SEM images are taken at 45 degrees angle. a) A single nano-particle from different arrays with the same period but different radii changing from 35–60 nm is collaged to give insight about the variation of the geometrical shapes with the applied dose. The scale bar is 100 nm. b) 60 nm radius array with period 200 nm. The scale bar is 300 nm. c) "Tandem" nanostructures. d) "Only gold" nanostructures.

collection fiber. The spectrum is then measured by Ocean optics USB4000 model spectrometer. The set-up is described schematically in **Figure 2**a.

To obtain the optical transmission characteristics background light intensity is firstly measured with the light source off. Then reference light intensity is measured with the light source on for an empty reference point, which means from the sapphire substrate with no nanocones. Finally the sample light intensity is measured as transmitted light at the presence of the nano-cone arrays under perpendicular illumination. The transmittance is the ratio of the sample light intensity to reference light intensity, where background noise is subtracted from both measurements. The measurement results are presented in Figure 2b along with the simulation results in Figure 2c.

2.3. FDTD Simulations

3D simulations are carried out on a single unit cell of the different sized arrays with a commercial "Finite-Difference Time-Domain Method" solver "Lumerical". The material data of Au is taken from the work of Johnson and Christy and for SiO_2 and sapphire from the work of Palik.[22,23] The truncated nanocones are illuminated by normal incidence from air side by a plane wave of frequency range 500–900 nm. The dimensions of the nanostructures are chosen in accordance with the physical sizes measured with SEM. The bottom radii of the truncated cones range from 45–60 nm whereas the heights are 30-15-30 nm for Au-SiO_2-Au layers respectively. Period is 200 nm and the cone angle is taken as 20°. The boundary conditions were set as perfectly matched layer (PML) in the direction of illumination to prevent undesired reflections from boundaries and periodic perpendicular to the direction of propagation. A mesh override region covering the nanostructures is used for fine resolution with high accuracy. The mesh sizes are set to 2 nm for transmission

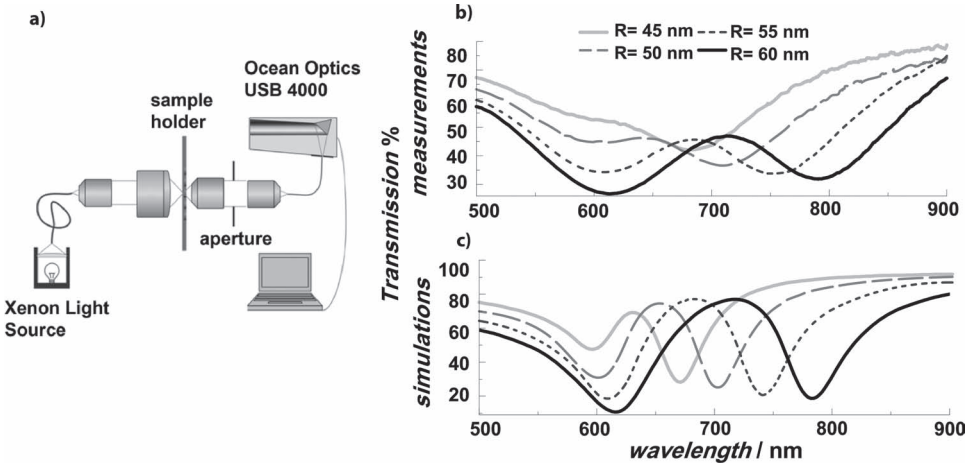

Figure 2. a) Transmission mesurements for the truncated nanocones. Period is 200 nm. Bottom radius vary from 45–60 nm, respective heights of the Au-SiO_2-Au layers are 30-15-30 nm. b) Simulation results for the similar sized arrays. c) Schematics of custom spectral transmission set-up.

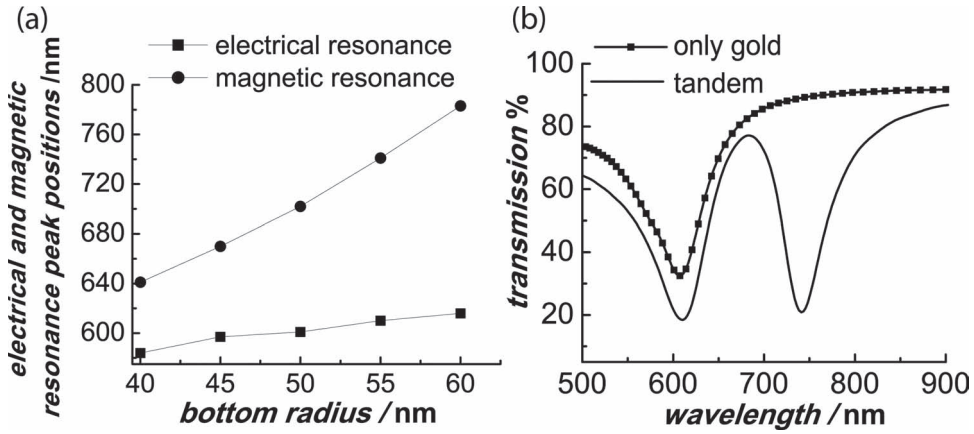

Figure 3. a) The variation of electrical and magnetic resonance peak positions with changes in bottom radius. Magnetic resonance is prone to changes in physical dimensions wheras the electrical resonance is not very sensitive. b) Simulated transmission spectra of the tandem and gold truncated nano cones used for comparison. Physical dimensions are illustrated in Figure 1c and d.

simulations whereas finer mesh sizes up to 0.25 nm is used for cross sectional monitors that depict E-field distributions.

The simulations are in agreement with the optical measurements in terms of resonance frequencies. The peaks at the shorter wavelengths have electric dipolar nature and is referred as electrical resonance whereas the peaks at the longer wavelengths have magnetic dipolar nature and referred as magnetic resonance.[16] Experimental data suffers from broadening due to possible fabrication imperfections such as size and/or shape dispersions however the positions of the resonance dips are closely matched.

It can be seen that the electrical resonances are not influenced much from diameter change at a fixed SiO_2 spacer thickness. However the magnetic resonance can be tuned by varying bottom radii as can be seen from **Figure 3**a. In SERS experiments usually a fixed wavelength laser is available and used for different molecules each exhibiting Stokes shifted Raman lines at different wavelengths. Such a design can aid to fix electrical resonance at the desired excitation wavelength and tune the other to match the tracked Raman line of the molecule under study. Such a tuning is possible by varying spacer thickness, too.[16]

For performance comparison gold truncated nanocones that have single resonance wavelength matched with the electrical resonance of tandem structures are simulated in accordance with the fabricated structures' dimensions. Their respective transmission spectra are shown in Figure 3b. The E-field distributions are drawn for both cases at the experimental excitation wavelength at 632 nm and at the tracked Raman line of benzenethiol under this illumination at 785 nm. Double resonance structures exhibit a higher E-field intensity at both wavelengths in "hot spots" formed at metal-dielectric boundaries. Also note that the in-phase dipolar moments at the electric resonance causes the magnetic field between the double resonance structures to vanish whereas the anti-phase dipolar moments at the magnetic resonance leads to the formation of a loop-like current that induces an intense magnetic field distribution.[16] On the other hand, single resonance gold structures exhibit poor E-field intensity at the Stokes shifted Raman line far from its resonance wavelength. This can be followed from the cross sectional electric field distributions provided in **Figure 4**. The figures also depict the spatial overlap of the enhanced fields for tandem structures

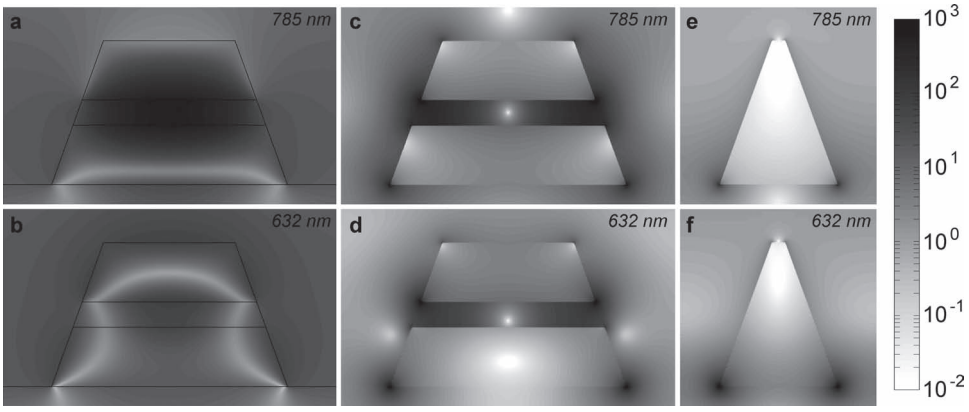

Figure 4. Cross sectional electric and magnetic field distributions (log ($|E|^2$), log ($|H|^2$)) of double and single resonance structures at raman shifted wavelength of tracked Raman line (785 nm) and at excitation wavelength (632 nm) where the resonance of gold nanostructures match the electrical resonance of tandem nanostructures. a,b) magnetic field distributions for double resonance structures. c,d) Electric field distributions for double resonance structures. e,f) Electric field distributions for single resonance. The dimensions are the same as indicated in Figure 1c and d. Same color bar is used for all figures except that for magnetic field a factor of 10^{-6} should be taken into account.

NANO MICRO small

at the two wavelengths that increases $|E_{excl}|^2$. $|E_{stokes}|^2$ and therefore the total electric field intensity.

The electromagnetic enhancement mechanism that is responsible for most of the resultant SERS enhancement relies on the intensity of the local electric field. Another simulation is done for the comparison of the electric field enhancements keeping all the previous settings. The electric field distribution is obtained for both cases at excitation and Stokes shifted wavelengths by 3D monitors. Then $|E_{excl}|^2$. $|E_{stokes}|^2$ is integrated over the exposed volume and normalized with the total surface area. The results for "tandem" structures with bottom disk radius of 60 nm and 50 nm are then compared with "only gold" structures with 30 nm radius at the same total height, in order to correlate with the SERS experiments. The resultant enhancement is about 16 for 60 nm radius array for the Raman line at 3054 cm^{-1} and about 9 for 50 nm radius array for the Raman line at 1075 cm^{-1}. The experimental values obtained for the same conditions are 11 for 60 nm radius array and for 10 for 50 nm radius array. The differences can be attributed to defects that may occur in fabrication stages such as lift off.

2.4. SERS Measurements

Packing density of benzenethiol is known and studied in previous reports. Therefore, it provides a good means for enhancement factor calculation and comparison with previously reported values. We have used the largest surface packing density reported for benzenethiol in the enhancement factor (EF) calculations (6.8×10^{14} molecules.cm^{-2}).[8,24,25] The homogenity was checked by taking several measurements from different spots on the same sensor area and the repetability of the measurements was found within error bound of ~13%. The measurements were taken right after coating.

The most common EF definition is used for comparison with similar structures that can be written as $EF = (I_{SERS}/N_{surf})/(I_{RS}/N_{vol})$.[8,9,26] Here, N_{vol} is the number of molecules in the detection volume that contribute to the Raman signal measured from neat, liquid benzenethiol and N_{surf} is the number of adsorbed molecules that contribute to the measured SERS signal. I_{RS} and I_{SERS} are the Raman and SERS intensities obtained from neat benzenethiol and the nano-lithographed SERS substrates, respectively.

In the Raman experiment, a thin glass container with neat benzenethiol is used. The probe volume was approximated as a cylinder of height that equals the thickness of neat benzenethiol following the same steps and reasoning as in the works of Chu and Banaee.[13,14] and calculated as 362 fl. The number of probed molecules is determined from $N_{vol} = NA\rho hA/M$ where NA is Avogadro's number, ρ is volume density (1.073 g cm^{-3}) and M is molar mass (110.18 g mol^{-1}) of benzenethiol molecules. h is the thickness of the neat benzenethiol sample and A is the spot area. N_{vol} calculated in this way is 2.1×10^{12} molecules.

In the SERS EF calculations, exposed gold surface area of a single truncated nano-cone is calculated using the SEM measured dimensions for every physically different array. Lateral and top surfaces are taken into account. Lateral surface area of the SiO_2 spacer is excluded from the total calculated area for tandem structures. The number of nanostructures at the spot area is calculated using the period of the truncated nanocones and spot size of the laser. A perfectly ordered self-assembled monolayer is assumed on the exposed surfaces to calculate maximum possible N_{surf}[8,24,25] Any possible defect at the exposed surfaces due to fabrication imperfections or in the monolayer formation would result in larger EF values. The calculation can be summarized as $N_{surf} = \rho_s S_{gold} A/P^2$ where ρ_s is the surface packing density, S_{gold} is the exposed gold area, A is the spot area and P is the period of the array.[13] Note that since the same objective is used in both Raman and SERS experiments, the spot area is actually cancelled out in the EF calculations.

To make a reasonable performance comparison, truncated gold nanocones that have single resonance wavelength that is matched with the electrical resonance of tandem structures are designed and fabricated. By this way one can observe the enhancement due to the presence of the second resonance with all the other conditions fixed. Baseline corrected SERS data is presented in **Figure 5**a for single resonance and tandem structures along with their optical transmission data. The physical dimensions and schematics of "tandem" and "only gold" structures are provided in Figure 1.

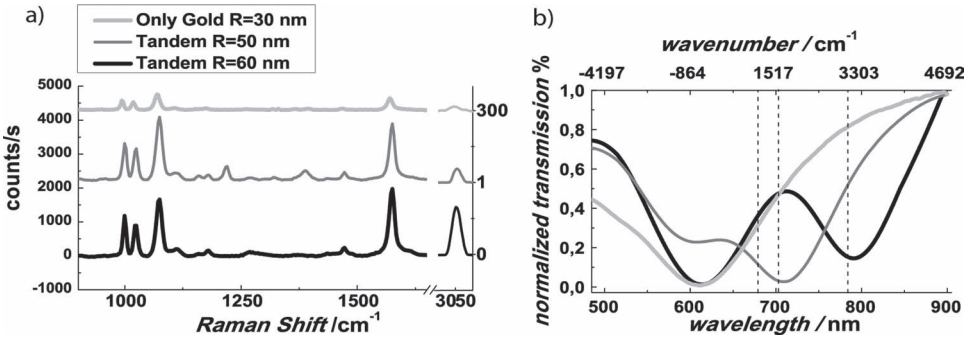

Figure 5. a) Baseline corrected SERS data from "tandem" and "only gold" nanostructures. An axis break is added to the horizontal axis for Raman line at 3055 cm^{-1} since this peak is both distant and not as intense as the other peaks. Spectra are shifted for a better view. b) Normalized transmission data for the same "tandem" and "only gold" nanostructures. The spectra is normalized to aid in the comparison of the position of the resonance wavelengths. The same legend applies to both figures. Raman Lines at 1075 cm^{-1}, 1575 cm^{-1} and 3055 cm^{-1} are indicated with dotted lines.

Table 1a. Calculated SERS Enhancement Factors for "tandem" and "only gold" arrays.

	3054 [cm^{-1}]	1575 [cm^{-1}]	1075 [cm^{-1}]
tandem R = 60 nm	7.12×10^5	2.20×10^7	2.52×10^7
tandem R = 50 nm	3.23×10^5	2.55×10^7	3.86×10^7
only gold R = 30 nm	6.38×10^4	2.51×10^6	3.80×10^6

Table 1b. Improvement of "tandem" with respect to "only gold" arrays.

	3054 [cm^{-1}]	1575 [cm^{-1}]	1075 [cm^{-1}]
tandem R = 60 nm	11×	9×	7×
tandem R = 50 nm	5×	10×	10×

As can be seen from Figure 5a Benzenethiol has characteristic raman lines at 999 cm^{-1}, 1024 cm^{-1}, 1075 cm^{-1}, 1575 cm^{-1}, and 3055 cm^{-1}. These lines correspond to the C–C–C in-plane ring-breathing mode, the in-plane C–H bending mode, the in-plane ring-breathing mode coupled with the C–S stretching mode, the C–C stretching mode and C–H stretching mode bonds of the molecule, respectively. The band at 3055 cm^{-1} is characteristically less intense than the others as observed in other studies that occupy gold substrates.[24] Therefore a different intensity scale is used after the axis break at 1750 cm^{-1} to be able to observe the variation at this Raman line especially for the truncated gold nanocones that have single resonance wavelength.

The optical transmission data presented in Figure 5b reveals that the magnetic resonance of the tandem structures with 50 nm bottom radius are tuned for 1000–1600 cm^{-1} and 60 nm bottom radius are tuned for 3055 cm^{-1}. The comparison between the proposed structures is done in terms of EFs to take into account the differences in exposed gold surface areas.

The variation in the calculated SERS EFs are presented in **Table 1.** In Table 1a, the EFs calculated for wavenumbers 1075 cm^{-1}, 1575 cm^{-1}, and 3055 cm^{-1} are presented for "tandem" and "only gold" arrays. In Table 1b, the ratios of the EFs for tandem structures to EFs for single resonance gold truncated cones are listed.

The double resonance "tandem" structures can provide roughly 10 times larger enhancement than single resonance "only gold" structures for the Raman shifted peaks closer to the magnetic resonance frequency for each of the tandem arrays. R = 60 nm array exhibits more than an order of magnitude enhancement for 3055 cm^{-1} line whereas R = 50 nm array exhibits a similar enhancement for 1075 and 1575 cm^{-1} lines. The obtained results are in accordance with the simulations and the theory.

3. Conclusion

In this study, a systematic tuning of the two resonance frequencies of tandem structures was done to maximize SERS EF. The maximum EFs obtained for Au-SiO_2-Au structures for 1075 cm^{-1} is 3.86×10^7. The double resonance structures were shown to provide 10-fold larger enhancement than their single resonance counterparts. This value can be further increased in applications such as NIR-SERS and SEHRS where the difference in frequency for excitation and scattering signals is more pronounced.

Gold was selected as the metal due to its chemical stability, biocompatibility and sharp resonance dip at the wavelengths under study. However it is reported in the literature that by using silver as the metal, one can further increase SERS enhancement.[13,27] So the enhancement values obtained in this study still has room for improvement simply by changing the type of metal.

Another way to increase the enhancement is to selectively etch some portion of the SiO_2 layer and the molecules that reside in this gap will experience a larger electric field than they do on the surface. The hot-spots formed in this way are expected to provide a larger enhancement that may even enable single molecule detection.

4. Experimental Section

Fabrication: For fabrication, an optically transparent sapphire substrate was chosen since tranmission measurements were planned for optical characterization. The sapphire substrate is spin coated with poly(methylmethacrylate) (PMMA 950 A-2) at 4000 rpm for 40 s. After pre-bake for 90 s at 180 °C, aqua-save (polymer) coating is done using the same parameters. "RAITH E-Line" system is used for lithography. The sample is developed at 1:3 MIBK:IPA (Methyl Isobutyl Ketone: Isopropyl Alcohol) developer for 40 seconds. The metal coating is done in "Leybold Univex 350 Coating System". The samples are kept in acetone for lift off for 5 minutes, and then the excess metal is lifted off with acetone flush.

SERS and Raman Experiments: The SERS data is collected by Horiba LABRAM Raman Spectrometer. The He-Ne excitation laser is 632.8 nm. The data is collected with 100× objective with 0.9 numerical aperture. The calculated spot size for the used objective is around 0.8 μm. Slit size of 200 μm and hole size of 1100 μm is used throughout the measurements. The data is collected with the same accumulation and exposure times for all samples.

Benzenethiol is purchased from Sigma, Aldrich and used as is in the Raman experiments. The substrates for SERS experiments are prepared by spin coating benzenethiol (10 mM) solution in ethanol, at 4000 rpm for 40 s. This provides a homogenous coating of the molecule on the different sensor areas residing at the middle of the same substrate.

Acknowledgements

This work is supported by the projects DPT-HAMIT, ESF-EPI-GRAT, NATO-SET-181 and TUBITAK under Project Nos., 107A004, 109A015, 109E301. One of the authors (E.O.) also acknowledges partial support from the Turkish Academy of Sciences. The authors thank A. Burak Turhan for his helps in fabrications.

[1] D. L. Jeanmaire, R. P. Van Duyne, *J. Electroanal. Chem.* **1977**, *84*, 1.
[2] M. G. Albrecht, J. A. Creighton, *J. Am. Chem. Soc.* **1977**, *99*, 5215.
[3] A. Campion, P. Kambhampati, *Chem. Soc. Rev.* **1998**, *27*, 241.
[4] C. L. Haynes, A. D. McFarland, R. P. Van Duyne, *Anal. Chem.* **2005**, *77*, 338a.
[5] P. L. Stiles, J. A. Dieringer, N. C. Shah, R. R. Van Duyne, *Annu. Rev. Anal. Chem.* **2008**, *1*, 601.
[6] M. Moskovits, *Rev. Mod. Phys.* **1985**, *57*, 783.
[7] E. Ozbay, *Science* **2006**, *311*, 189.
[8] C. L. Haynes, R. P. Van Duyne, *J. Phys. Chem. B* **2003**, *107*, 7426.
[9] A. D. McFarland, M. A. Young, J. A. Dieringer, R. P. Van Duyne, *J. Phys. Chem. B* **2005**, *109*, 11279.
[10] A. Wokaun, *Solid State Phys.* **1984**, *38*, 223.
[11] J. Grand, M. L. de la Chapelle, J. L. Bijeon, P. M. Adam, A. Vial, P. Royer, *Phys. Rev. B* **2005**, *72*, 33407.
[12] E. C. Le Ru, P. G. Etchegoin, *Chem. Phys. Lett.* **2006**, *423*, 63.
[13] Y. Z. Chu, M. G. Banaee, K. B. Crozier, *Acs Nano* **2010**, *4*, 2804.
[14] M. G. Banaee, K. B. Crozier, *ACS Nano* **2011**, *5*, 307.
[15] Y. Jeyaram, S. K. Jha, M. Agio, J. F. Loffler, Y. Ekinci, *Opt. Lett.* **2010**, *35*, 1656.
[16] Y. Ekinci, A. Christ, M. Agio, O. J. F. Martin, H. H. Solak, J. F. Loffler, *Opt. Express* **2008**, *16*, 13287.
[17] P. Hendra, C. Jones, G. Warnes, *Fourier Transform Raman Spectroscopy: Instrumentation and Chemical Applications*. Horwood, New York **1991**.
[18] S. Mahajan, M. Abdelsalam, Y. Suguwara, S. Cintra, A. Russell, J. Baumberg, P. Bartlett, *Phys. Chem. Chem. Phys.* **2007**, *9*, 104.
[19] J. C. Hulteen, M. A. Young, R. P. Van Duyne, *Langmuir* **2006**, *22*, 10354.
[20] N. A. Cinel, S. Butun, *Opt. Express* **2012**, *20*, 2587.
[21] A. Baba, A. Kaya, N. Turk, *J. Appl. Sci.* **2005**, *5*, 800.
[22] P. B. Johnson, R. W. Christy, *Phys. Rev. B* **1972**, *6*, 4370.
[23] E. D. Palik, *Handbook of Optical Constants of Solids*. Academic Press, San Diego **1998**.
[24] L. J. Wan, M. Terashima, H. Noda, M. Osawa, *J. Phys. Chem. B* **2000**, *104*, 3563.
[25] C. M. Whelan, M. R. Smyth, C. J. Barnes, *Langmuir* **1999**, *15*, 116.
[26] E. C. Le Ru, E. Blackie, M. Meyer, P. G. Etchegoin, *J. Phys. Chem. C* **2007**, *111*, 13794.
[27] D. A. Genov, A. K. Sarychev, V. M. Shalaev, A. Wei, *Nano Lett.* **2004**, *4*, 153.

Received: June 11, 2012
Revised: August 22, 2012
Published online: October 12, 2012